NANO · MICRO small
www.small-journal.com

Multiscale Engineering of Nanofiber-Aerogel Composite Nanogenerator with Tunable Triboelectric Performance Based on Multifunctional Polysuccinimide

Mirae Kim, Cholong Choi, Jin Pyo Lee, Jiyun Kim, and Chaenyung Cha**

Multiscale polymer engineering, involving chemical modification to control their triboelectric polarities as well as physicomechanical modification to maximize charge transfer and structural durability, is paramount to developing a high-performance triboelectric nanogenerator (TENG). This report introduces a highly efficient and comprehensive strategy to engineer high-performance TENG based on multifunctional polysuccinimide (PSI). With the ability of PSI to undergo facile nucleophilic addition with amines, sodium sulfate and quaternary ammonium chlorides having opposite charged groups are conjugated to PSI in varying densities. The resulting Sulfo-PSI and TMAC-PSI, respectively, processed into nanofibrous films, demonstrate highly enhanced and variable triboelectric properties based on the charge type and density. To further enhance the mechanical toughness and biocompatibility necessary for wearable applications, these PSI nanofibers are processed into alginate aerogel (AG). The sustained triboelectric performance of this nanofiber-AG TENG as a wearable energy harvester and biosensor is examined and validated in detail.

1. Introduction

With the rise of portable electronics and wearable biomedical devices, there is a growing need to find a light-weight, sustainable, and miniaturized energy source for durable operation. In addition to rechargeable batteries, it is highly desired to integrate energy harvesting systems utilizing largely discarded and ambient energy sources, such as electromagnetic radiation (photovoltaic), residual heat (thermoelectric), and mechanical forces (piezoelectric).[1–4]

Recently, triboelectrification, in which electrostatic charges with opposite signs are transferred between materials with contrasting charge affinities, has gained significant attention for applications in energy harvesting and sensor devices.[5–8] Commonly referred as triboelectric nanogenerators (TENGs), TENGs have several advantages, such as wide material selection, cost effectiveness, simple device design, and high energy conversion efficiency and power output.[9–11] For a typical set-up, a pair of materials with different surface electrical potentials, an electron donor layer and an electron acceptor layer, are allowed to contact each other, resulting in charge generation and transfer.

In order to achieve the maximum surface charge density for high-performance TENGs, it is important to develop a dielectric material with high permittivity that can effectively can effectively lead strong internal polarization enhancing the charge induction upon physical contact. For this reason, a wide range of well-known polymers, both synthetic and natural, have been generally chosen for TENG operation, which are widely tabulated into "triboelectric series" based on triboelectric polarity.[9,10] For example, polytetrafluoroethylene (PTFE), perfluoroalkoxy alkane (PFA), poly(vinylidene fluoride) (PVDF), polydimethylsiloxane (PDMS), and Kapton, which contain extensive amounts of electronegative elements (e.g., fluorine and oxygen) or electron-withdrawing groups (e.g., phthalimide), are mostly used as electron acceptors. While metals (e.g., aluminum (Al), copper, and silver) are widely used as electron donors, polymers such as polyamides (e.g., Nylon) and biological tissues mostly consisting of proteins that contain electron-donating amides, have been also used as electron donors. Since most TENGs are developed by choosing and matching known materials, it is difficult to precisely control the triboelectric output. Therefore, research efforts are underway to chemically engineer polymers with various functional moieties in order to augment and control their triboelectric properties.[12–14]

Since the triboelectric charge is transferred via physical contact, physicomechanical properties of polymers that influence the degree of interaction between two materials, such as surface topography, elasticity, and porosity, are also important parameters for developing TENGs. For this purpose, several strategies to introduce nano- and micro-scale structures, such as lithography and composite formation, have been adopted.[15–19] It is also important to maintain their structural integrity and mechanical strength in order to maintain repeated usages, which is often the prime reason for selecting a particular material, aside from triboelectric polarity. For example, fluorinated polymers or polysiloxanes are largely selected not only for high electron-withdrawing effect, but also their high mechanical strength, durability, and even stretchability. Other

M. Kim, C. Choi, J. P. Lee, J. Kim, C. Cha
Center for Multidimensional Programmable Matter
Department of Materials Science and Engineering
Ulsan National Institute of Science and Technology (UNIST)
Ulsan 44919, Republic of Korea
E-mail: jiyunkim@unist.ac.kr; ccha@unist.ac.kr

The ORCID identification number(s) for the author(s) of this article can be found under https://doi.org/10.1002/smll.202107316.

DOI: 10.1002/smll.202107316

polymers such as Nylon and poly(ethylene terephthalate) (PET) that are cost-effective and mechanically tough but have relatively low triboelectric polarities have also been widely used for this reason. Despite various engineering strategies developed and implemented for TENG technology, they are mostly disparate approaches, tied to a specific material or device. However, it is more desirable to employ a more universal engineering strategy that could be applied to a variety of TENG systems in order to more precisely control their triboelectric performances.

This study provides a comprehensive engineering strategy to both (1) control the triboelectric polarity with a multifunctional polymer capable of facile chemical modification and (2) provide highly biocompatible, mechanically conformal and durable TENG platform via nanofiber-aerogel composite system (**Figure 1**). Polysuccinimide (PSI) consists of a series of asymmetric succinimidyl moieties which possess dynamic electronic resonance states, and has been demonstrated to undergo electrical polarization.[20] Moreover, they are capable of undergoing ring-opening addition with amine-based nucleophiles.[9,21] This unique feature of PSI was utilized to conjugate charged functional groups, sodium sulfate (Sulfo-PSI) or quaternary ammonium chloride (TMAC-PSI), in varying degrees. It was expected that the triboelectric charge affinities of Sulfo-PSI and TMAC-PSI would be widely varied based on their degrees of substitution. Furthermore, they were processed into mechanically-durable nanofibrous films for prolonged triboelectric operations.

In order to fabricate a more conformal and shape-recoverable TENG platform for wearable biomedical devices, the PSI nanofibers were cut into short, dispersible form and infused within a biocompatible alginate aerogel. Due to the unique physicomechanical properties of aerogels (e.g., lightweight, mechanical conformity and toughness, high porosity and surface area), aerogels are widely considered an attractive platform for wearable and biomedical devices.[22–25] By incorporating triboelectric nanofibers into aerogels, it was expected that the triboelectric properties could independently imparted and controlled by varying the nanofiber concentration within the aerogel. The mechanical and triboelectric properties of the nanofiber-laden aerogels were systematically examined to assess their potential as a wearable energy harvesting device.

2. Results and Discussion

2.1. Synthesis and Characterization of Functional PSI

PSI is comprised of a series of succinimidyl groups. Imide contains two acyl groups separated by nitrogen, which makes it capable of forming multiple resonance structures. Coupled with the presence of electronegative oxygen and nitrogen, it was expected that PSI could be induced to have a considerable electric polarity. Furthermore, the succinimidyl groups can undergo ring-opening nucleophilic addition with amine-based molecules. This unique feature of PSI has been widely explored to present a variety of functional moieties.[21] In this study, two different ionic groups, anionic sodium sulfate and cationic quaternary ammonium chloride, were introduced to PSI, namely Sulfo-PSI and TMAC-PSI, respectively. It has been well established that ionic groups have the capability of effective charge transfer, and thus, it was hypothesized that opposite triboelectric potentials would be demonstrated between Sulfo-PSI and TMAC-PSI.[26]

Sulfo-PSI and TMAC were synthesized by reacting PSI with Sulfo-NH_2 and TMAC-NH_2 (Figure 1a). The degrees of substitution for Sulfo-PSI (DS_{Sulfo}) and TMAC-PSI (DS_{TMAC}) were

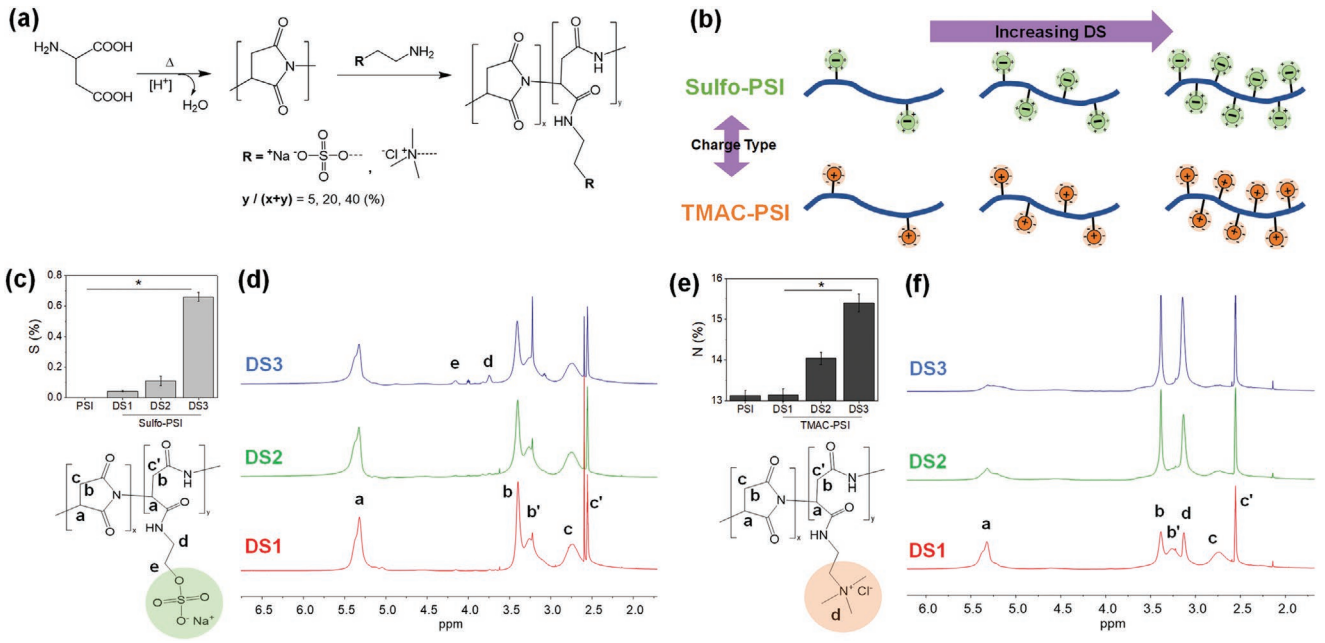

Figure 1. a) Synthesis of polysuccinimide (PSI) and its derivatization to present sodium sulfate (Sulfo) or trimethylammonium chloride (TMAC). b) The electrical potential of PSI was controlled by varying the degree of substitution (DS) of Sulfo or TMAC groups. Elemental analyses (sulfur and nitrogen) and ^{1}H-NMR spectra of c,d) Sulfo-PSI and e,f) TMAC-PSI with varying DS.

conveniently controlled by varying the feed ratio of the reactant to PSI. Three different DS's were prepared; 5%, 20%, 40% of succinimidyl groups in PSI, termed DS1, DS2, and DS3, respectively. The maximum DS was chosen as 40%, as any DS above this range led to aqueous dissolution, which is not desirable for use as TENG, due to the loss of hydrophobic succinimidyl groups and the generation of hydrophilic functional groups. ^{1}H-NMR and FT-IR spectra confirmed the increasing presence of functional groups (Figure 1c,e; Figure S2, Supporting Information). Furthermore, elemental analyses also showed the increasing presence of sulfur and nitrogen for Sulfo-PSI and TMAC-PSI, respectively (Figure 1d,f).

2.2. Fabrication and Triboelectric Measurement of PSI Nanofibrous Film

To evaluate the triboelectric potential of PSI, it was first processed into a film by solvent casting. However, due to the mechanical weakness of PSI, despite using the highest molecular weight possible for PSI at 70 kDa, the films were brittle and easily broken upon mechanical loading (data not shown). The inability to stably generate higher molecular weight chain that is crucial for mechanical durability is a major drawback of PSI.[27] To overcome this issue, PSI was processed into nanofibrous film, which has the advantage of increased surface area for greater contact, as well as increased mechanical strength.[28]

Nanofibers were fabricated by electrospinning. To optimize the nanofibers that provide the maximal mechanical strength upon repeated mechanical loading for contact-separation measurements, the morphology was controlled by adjusting the concentration of PSI solution for electrospinning (**Figure 2**a). The nanofiber began to form at 20%, where there was a significant presence of particulates within the nanofiber, demonstrating that the polymer concentration was not high enough to form cohesive fibers, and solvent was not effectively evaporated (i.e., this condition was closer to electrospraying than electrospinning). As a result, the film was extremely brittle. At 25%, nanofiber was more stably formed without any noticeable particulates. However, after repeated mechanical loading, lint was generated from the surface, which signified the lack of mechanical strength, possibly arising from lack of fiber length and density.

At higher PSI concentration of 30%, the structural integrity of PSI nanofiber film was well maintained without any deterioration even after repeated mechanical loading. As shown in the scanning electron microscopic (SEM) image, there was a greater presence of interconnected nanofibers and beaded fibers, compared to those generated at lower concentrations, which is often attributed to the instability of polymer jet during electrospinning, especially for fluids with higher viscosity.[29] These structurally irregularities had a reinforcing effect on the nanofiber film, in which the bead acted as a point of fusion, anchoring nanofibers together to impart significantly enhanced mechanical strength.[30] This condition, therefore, was used for all triboelectric measurements. It should be noted that the viscosity of PSI solution above 30% became critically high that nanofiber could not be generated even at higher voltage.

The triboelectric potentials of the PSI and functional PSI were then examined. As-fabricated PSI nanofibrous layers were tested against a PFA layer, a widely-used triboelectric material with high electron-withdrawing effect (Figure 2b; Video S1, Supporting Information), and the resulting output open-circuit voltage (V_{OC}) and short-circuit current (I_{SC}) were measured (Figure 2c,d). Al, which is a well-known electron-donating material, was used as a reference. It was clearly evident that Sulfo-PSI showed much greater V_{OC} than TMAC-PSI. The V_{OC} continued to increase with DS_{Sulfo} that it became even larger than that of Al at the highest DS_{Sulfo} (DS3). On the other hand, the V_{OC} of TMAC-PSI was much lower than that of Al. The trend for I_{SC} generally coincided well with that of V_{OC}, which demonstrated that continuously accumulated charge by triboelectrication was effectively transferred out to the connected circuit. Taken together, the contrasting triboelectric performances of Sulfo-PSI and TMAC-PSI clearly highlighted that sodium sulfate demonstrated substantial electron-donating effect due to the presence of electron-rich sulfonyl groups, while electron-deficient trimethylammonium showed the opposite effect.

The power output of the PSI TENG with variable load resistances, ranging from 100 KΩ to 10 MΩ was also measured (Figure 2e; Figure S3, Supporting Information). As expected, the power density remained low for TMAC-PSI regardless of load resistance (Figure S3d, Supporting Information). The power densities of PSI and Sulfo-PSI, on the other hand, increased with load resistance, similar to Al, up to 1 MΩ. However, above 1 MΩ, the power density for Al decreased due to a significant decrease in current by the ohmic loss (Figure S3a, Supporting Information). However, for PSI and Sulfo-PSI, the power densities remained high, even showed further increase for Sulfo-PSI. This result signified that the increase in voltages for PSI and Sulfo-PSI was significantly higher than that of Al, which could compensate for the ohmic current loss, even at high load resistances (Figure S3b,c, Supporting Information).

It is noteworthy to point out that PSI itself, even without charge functionalization, was shown to possess substantial triboelectric potential, as evidenced by even higher V_{OC} than Al. It was a surprising result given the extensive presence of imide moieties which are generally known for electron-withdrawing effect, as shown for Kapton.[31,32] Unlike Kapton which consists of aryl imides, in which partial charge on carbonyl groups are delocalized and stabilized by resonance, succinimide in PSI, devoid of resonance, possibly showed more ionic character on the carbonyl groups. Therefore, the succinimidyl rings in PSI were structurally similar and imparted similar electron-donating effect as amide bonds in proteins.[33–35]

Because of high electron-donating effect of PSI, V_{OC} showed decrease at the lowest DS_{Sulfo} (DS1) of Sulfo-PSI, as the elimination of a small amount of succinimidyl groups and the subsequent loss of triboelectric potential outweighed the triboelectric gain by sodium sulfate. However, the subsequent increase in V_{OC} at higher DS_{Sulfo} than PSI indicated that a sufficient amount of sodium sulfate groups could generate much greater electron-donating effect than PSI. Moreover, the high electron-donating effect of PSI is also the reason for decreasing V_{OC}

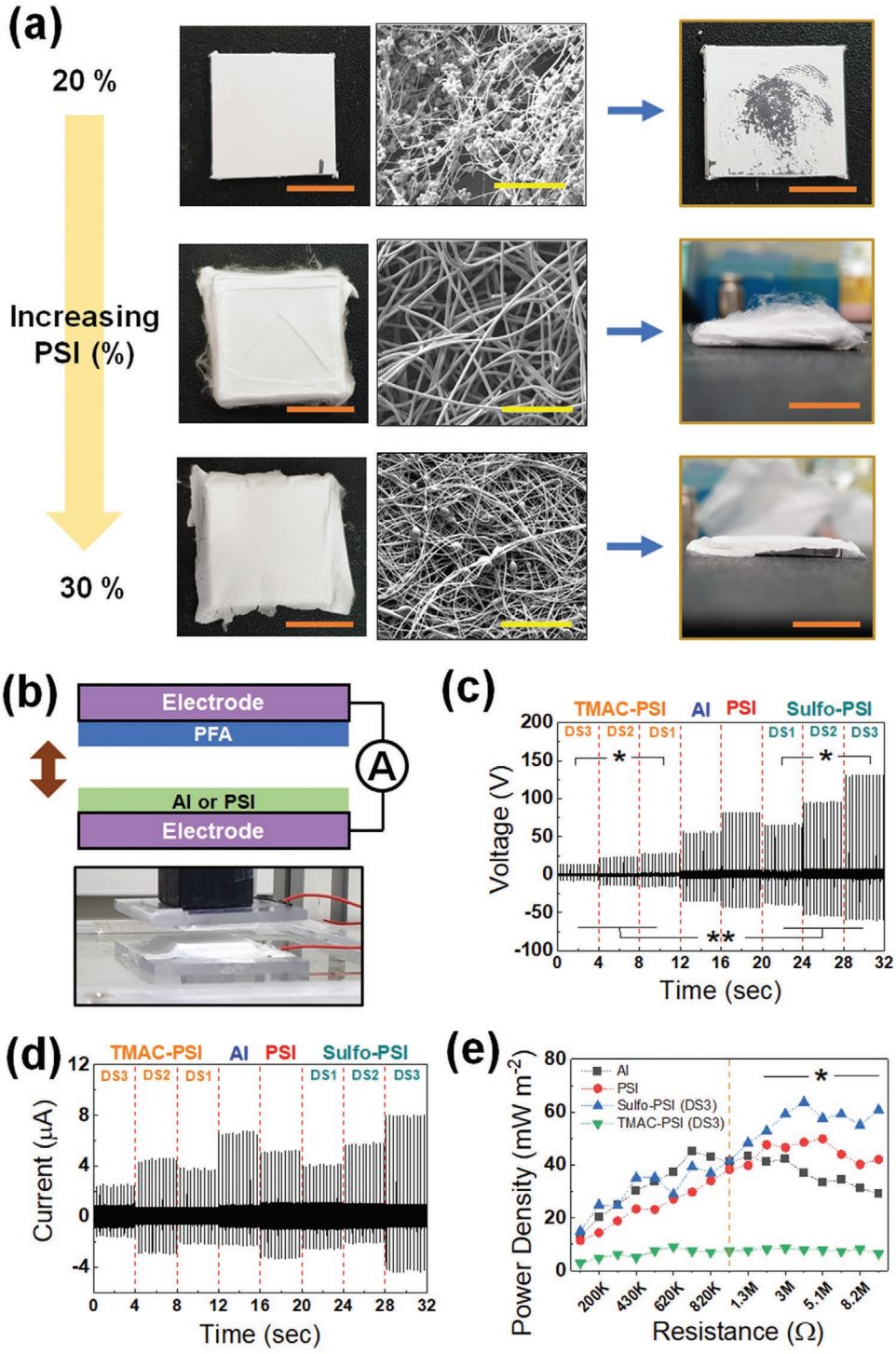

Figure 2. a) Photographs and scanning electron microscopic (SEM) images of PSI nanofibrous films developed by electrospinning at different PSI concentrations; 20%, 25%, and 30% w/v, from top to bottom (scale bar: 1 cm for photographs, 30 μm for SEM images). Photographs on the right show the films after repeated mechanical loading. b) Schematic illustration and photograph of PSI nanofiber TENG in a contact-separation mode. c) Open-circuit voltage and d) short-circuit current of TENG were measured with PSI, Sulfo-PSI, and TMAC-PSI layers against PFA layer (*$p < 0.05$ at $n = 10$ comparing different DS_{Sulfo}'s and DS_{TMAC}'s, **$p < 0.01$ at $n = 10$ comparing Sulfo-PSI and TMAC-PSI at the same DS). Aluminum (Al) layer was used as a reference material. e) The power densities measured with varying external load resistances, controlled from 100 kΩ to 10 MΩ (*$p < 0.05$ at $n = 10$ at the same resistance).

of TMAC-PSI increasing DS_{TMAC}. The increasing presence of electron-deficient TMAC likely negated the electron-donating effect of electron-rich PSI. Overall, PSI and its charged derivatives have demonstrated significant and variable triboelectric performance based on their degrees of substitution of charged groups.

2.3. Fabrication and Characterization of Nanofiber-Laden Aerogel

Aerogels are highly porous and flexible materials, having extremely low density and high surface area. Their solid structures are made by physical or chemical crosslinking of a variety of polymers and nano- and microstructures. For example, silica aerogels are commonly developed by sol-gel method followed by supercritical drying.[36] Natural polysaccharides have also been widely used to generate aerogels, due to their ability to undergo facile gelation and tunable mechanical properties via electrostatic interactions (e.g., alginate, κ-carrageenan, and chitosan), or hydrogen bonding (e.g., agarose).[37] These aerogels made from biocompatible materials are actively explored in biomedical and environmental applications, such as drug delivery systems, biosensors, and environmental remediation.[24,38,39]

In order to create a miniaturized device with high wearability, it is highly desirable to assemble a device on a lightweight, mechanically conformal and biocompatible material platform.[40] For this reason, physicomechanical properties of aerogel made from biocompatible materials are considered highly attractive and increasingly utilized.[37,41] Herein, aerogel was used as a three-dimensional TENG platform to incorporate PSI nanofibers for having extremely low dielectric constants with high surface area, in addition to aforementioned physicomechanical properties.[23] Low dielectric properties of aerogel means the embedded nanofibers can impart and transfer triboelectric charge without significant loss of charge to the surrounding aerogel network. The high surface area of aerogel also allows greater area of contact for TENG operation and increased available space for nanofiber inclusion. In this study platform for their favorable physicomechanical properties. It also served as a composite matrix that could incorporate PSI nanofibers for enhanced triboelectrification.

2.3.1. Physicomechanical Properties

Alginate aerogel was prepared by first Ca^{2+} crosslinking of alginate solution to fabricate hydrogel, followed by supercritical drying (**Figure 3**a). The nanofiber-laden aerogels (nanofiber-AG) were fabricated by dispersion of short PSI nanofibers, developed ultrasonic cutting of electrospun nanofibers, within the alginate network. Aerogel without nanofiber ("AG"), aerogels infused with PSI nanofiber ("PSI AG"), Sulfo-PSI nanofiber ("Sulfo-PSI AG"), and TMAC-PSI nanofiber ("TMAC-PSI AG") were prepared. The photograph and SEM images clearly showed the highly porous network, with nanofibers integrated into the alginate network (Figure 3b). The increasing amounts of nanofibers are clearly demonstrated. Furthermore, the surface roughness of the pore wall became substantially increased by the increasing presence of nanofibers. The pore diameters measured from the SEM images decreased with nanofiber concentration (Figure 3c). Interestingly, the pore diameter continued to decrease with PSI concentration, they increased again at 4% Sulfo-PSI and TMAC-PSI. It is believed that increasing presence of hydrophobic PSI within hydrophilic alginate network led to the structural collapse, while ionic Sulfo-PSI and TMAC-PSI could more favorably interact with alginate and push the pore walls apart.

The mechanical properties of the nanofiber-AGs were assessed by measuring Young's moduli from uniaxial compression (Figure 3d). Incorporating nanofibers into aerogel resulted in increased rigidity, regardless of nanofiber type. Coupled with decreasing pore size, this result confirmed the mechanical reinforcing effects of the nanofiber on the alginate network. Notably, the increase in moduli with nanofiber concentration was much more pronounced for both Sulfo-PSI AG and TMAC-PSI AG having opposite charges, which alluded to the different kinds of electrostatic interaction with alginate network. For Sulfo-PSI, the negative charge of sulfate allowed Sulfo-PSI to undergo ionic crosslinking with Ca^{2+} along with alginate.[42] For TMAC-PSI, on the other hand, positively-charged TMAC reinforced alginate network by directly interacting with alginate. Given the higher moduli of TMAC-PSI AG than Sulfo-PSI AG at the same nanofiber concentration, it could be reasoned that the polyelectrolyte interaction between alginate and TMAC-PSI was more effective for enhancing the mechanical properties than the additional ionic crosslinking of Sulfo-PSI by Ca^{2+}.

2.3.2. Triboelectric Properties

The triboelectric properties of nanofiber-AG TENGs were evaluated by measuring V_{OC} and I_{SC} against PFA via contact-separation mode, as similarly done with nanofibrous films (**Figure 4**a–1; Video S2, Supporting Information). The alginate aerogel itself did not demonstrate significant triboelectric charge induction, showing lower V_{OC} than Al and all the nanofiber-AGs, which clearly showed the limited electron-donating effect of natural polysaccharides.[9] However, the V_{OC} increased significantly with nanofiber concentration for PSI AG and Sulfo-PSI AG (Figure 4b,c). While the maximum V_{OC} was achieved at 2% PSI and did not increase further at 4%, there was a gradual increase in V_{OC}, reaching the maximum value at 4% for Sulfo-PSI AG. For TMAC-PSI AG, there was a small increase in V_{OC} up to 2% nanofiber, but decreased sharply at 4%. These results all closely followed the trends of V_{OC} measured for nanofiber films in Figure 2, which clearly illustrated that the triboelectric polarities of different PSI nanofibers could be effectively imparted within the aerogel platform.

It is worth noting that there was a clear difference in the preferential direction of the output peaks, often called "asymmetric output," between nanofibrous films and nanofiber-AGs, which is often observed in a vertical contact-separation mode.[43,44] For nanofibrous films, the asymmetric output showed much greater bias towards positive peaks ("positive asymmetric output") for both V_{OC} and I_{SC} (Figure 2). On the other hand, for nanofiber-AGs, the asymmetric output of V_{OC} was greatly diminished with increasing nanofiber concentration (Figure 4b–d). Surprisingly, the asymmetric output of I_{SC} was more biased towards negative peaks ("negative asymmetric output"), especially for nanofiber-AGs at lower nanofiber concentrations (Figure 4e,f). These results highlight the difference in mechanical properties between thinner nanofibrous film and thicker and deformable aerogel.[44] For nanofibrous films, the initial contact and subsequent separation occurred more readily without significant drag caused by adhesive force against PFA layer, thereby quickly transferring triboelectric

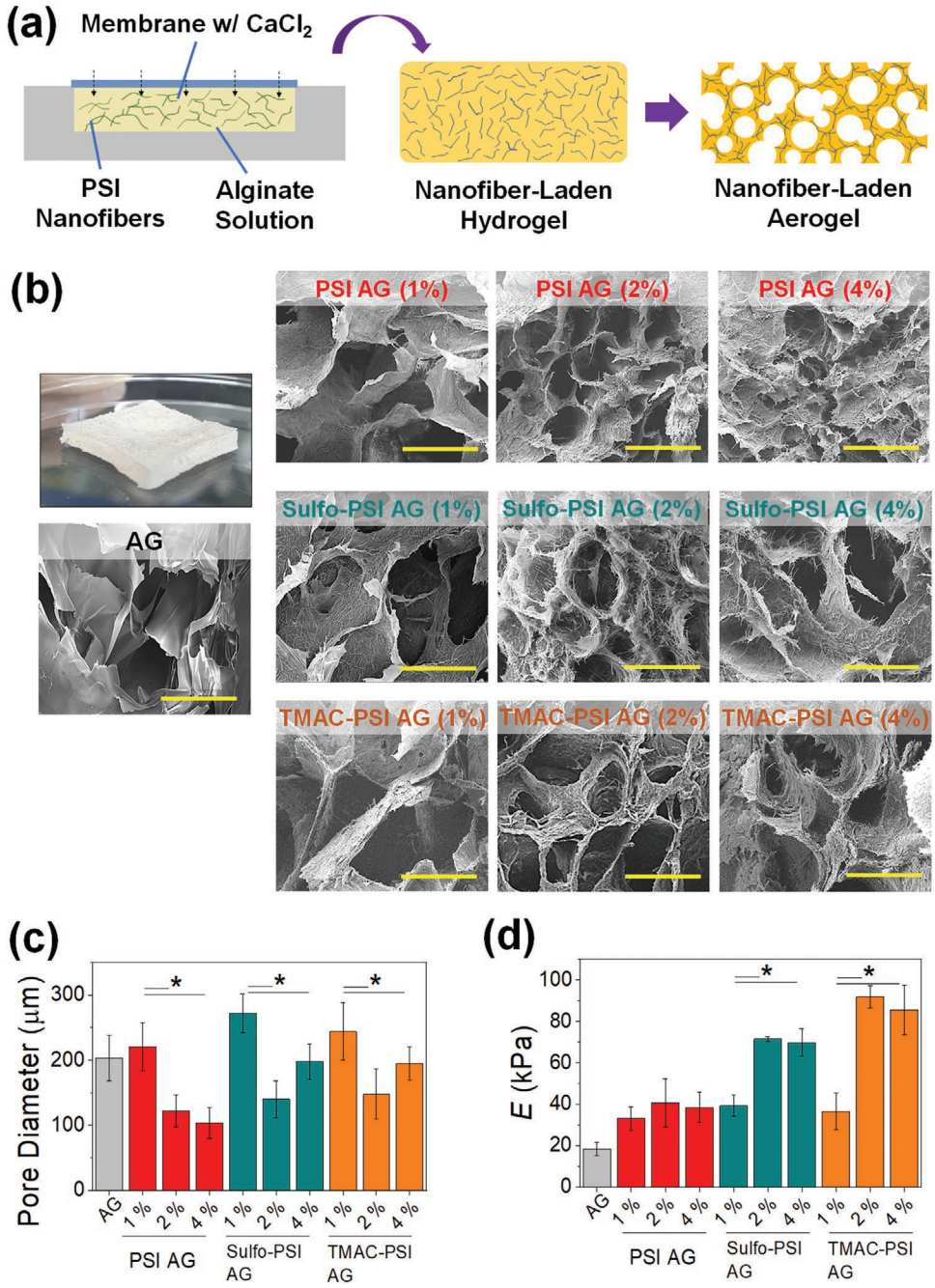

Figure 3. a) Schematic illustration of developing nanofiber-laden aerogels (nanofiber-AG). b) Morphological features of nanofiber-AG were examined by SEM; AG, PSI AG, Sulfo-PSI AG, and TMAC-PSI AG (scale bar: 200 μm). The nanofiber concentration was controlled up to 4%. c) Pore diameters and d) Young's moduli of the nanofiber-AGs (*$p < 0.05$ at $n = 10$ comparing different nanofiber concentrations).

charge leading to a sharp peak in the positive direction. With greater charge affinity of PFA, the recovery of tribo-charge upon the following contact was slower, leading to short and broader peak in the negative direction. For nanofiber-AGs, there is a substantial mechanical deformation (compression) due to the high mechanical conformity and thickness of aerogels. As a result, there was a time lag during shape recovery upon separation, causing a difference in ascending and descending motion (i.e., quicker contact and slower separation). Therefore, the slower separation meant attenuated triboelectric potential generation.

While V_{OC}'s of AG and nanofiber-AG at 1% nanofiber were lower than those of nanofiber-AG at higher nanofiber concentration, their overall intensities of I_{SC}'s did not significantly differ, but showed the opposite negative asymmetric I_{SC} output. This interesting phenomenon suggested that significant amount of tribo-charge generated by nanofiber remained within the aerogel. As shown by low V_{OC} against PFA, the aerogel

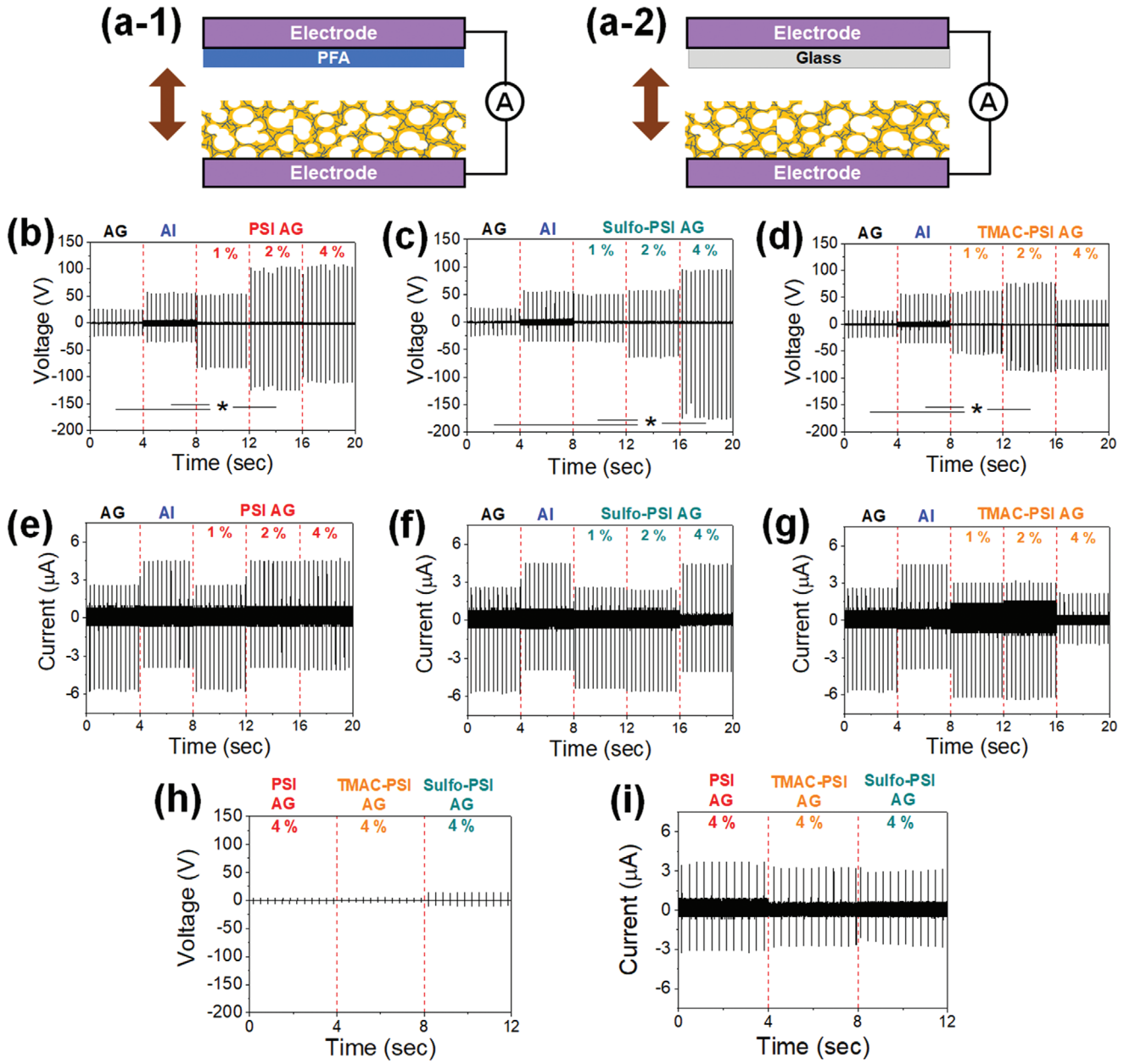

Figure 4. a) Schematic illustration of nanofiber-AG TENG in a contact-separation mode measured against PFA or glass. b–d,h) Open-circuit voltage and e–g,i) short-circuit current values of PSI AG, Sulfo-PSI AG, and TMAC-PSI AG were measured against b–g) PFA or h,i) glass (*$p < 0.05$ at $n = 10$ comparing different nanofiber concentrations). Al was used as a reference material. The nanofiber concentration was controlled up to 4%.

itself is an effective tribo-positive material (electron acceptor). Therefore, the tribo-charge was generated by contact with not only PFA, but also surrounding aerogel network, which in turn increased I_{SC} in the opposite direction. However, this negative asymmetric output was largely eliminated at higher nanofiber concentration, suggesting that increased amount of nanofibers could directly contact and transfer the tribo-charge to the PFA layer.

To further confirm the triboelectric potentials of PSI and its derivatives, V_{OC} and I_{SC} were measured against glass (Figure 4a-2). Since glass is one of the most tribo-positive (electron-donating) materials, opposite to PFA, it was hypothesized that triboelectric potential would be highly diminished for PSI-based materials which were also shown to be highly electron-donating. As expected, V_{OC} values of PSI AG, TMAC-PSI AG, and Sulfo-PSI AG all were critically diminished (Figure 4h). Furthermore, the initial direction of V_{OC} peak upon contact was negative for PSI AG and TMAC-PSI AG, which was opposite to those against PFA, indicating they were even more tribo-positive than glass. I_{SC} values of PSI AG and Sulfo-PSI AG did became lower, but those of TMAC-PSI AG were not significantly affected by glass substrate (Figure 4i). This opposite effect highlighted that TMAC-PSI having greater electron-withdrawing effect than PSI and

Sulfo-PSI could better accommodate electron transfer from glass.

Load resistance was also controlled and the resulting power densities were measured for the aerogel and nanofiber-AGs (Figure S4). Aerogel itself produced the lowest output power densities at all load resistances, as expected. Similar to the nanofibrous films, nanofiber-AGs showed much greater power densities at higher load frequencies than those of Al and aerogel. TMAC-PSI AG showed the smallest increase in power density, while PSI AG and Sulfo-PSI AG showed much larger increase in power density. For both PSI AG and Sulfo-PSI AG, the maximal power densities were measured at an intermediate resistance of 2 MΩ, indicating the current became critically diminished at higher resistance. Another significant finding is that the power densities at various load resistances were generally higher for nanofiber-laden hydrogels than nanofibrous films. For example, the maximal power densities for the nanofiber-laden hydrogels increased from 130 to 225 mW m^{-2} at 2 MΩ for Sulfo-PSI AG with nanofiber concentrations, while it was 65 mW m^{-2} at 4.7 MΩ for Sulfo PSI. This result signified that the amount of nanofibers within the aerogel was much greater than the nanofibrous film that the triboelectric charging could be more stably maintained at higher load resistances.

Different triboelectric polarities of PSI nanofiber-AGs were further examined by measuring V_{OC} and I_{SC} of aerogel-only TENG, consisting of different pairs of nanofiber-AGs; PSI AG with Sulfo-PSI AG, PSI AG with TMAC-PSI AG, and Sulfo-PSI AG with TMAC-PSI AG (**Figure 5**a). Due to the low triboelectric potential of aerogel, the overall V_{OC} and I_{SC} remained much lower than those obtained against PFA, regardless of nanofiber concentrations. However, there were clear differences in V_{OC} and I_{SC} when different nanofiber-AGs were paired. The V_{OC} of Sulfo-PSI AG against TMAC-PSI was much larger than those of PSI AG against Sulfo-PSI AG and TMAC-PSI AG (Figure 5b). This result clearly showed the opposite triboelectric polarities of Sulfo-PSI AG and TMAC-PSI AG, in line with the results obtained against PFA. I_{SC} was also the highest for Sulfo-PSI AG against TMAC-PSI (Figure 5c). Interestingly, there was an even larger extent of triboelectric bias for these aerogel-only TENG than those shown for the aerogels against PFA, which further signified the difficulty of efficient charge transfer for aerogels, which leads to more preferential charge accumulation within the aerogel than charge transfer. Nevertheless, triboelectric charge induction could be effectively controlled with different PSI nanofibers even within the aerogel platform. Taken all together, functional PSI nanofibers either in film or in aerogel allowed highly efficient fabrication and demonstrated substantial and tunable triboelectric performance.

2.3.3. Mechanical Durability

TENGs are operated under constant mechanical force, so it is important for them to possess high mechanical durability in order to maintain their structural integrity and functions for a long period of time. To demonstrate the mechanical durability of nanofiber-AGs, they were subjected to repeated contact-separation cycles with a considerable force. Since aerogels are highly flexible, they showed excellent shape recovery after mechanical loading up to 1000 cycles, and did not show any structural disintegration (Video S2, Supporting Information). With continued operation up to 10 000 cycles, the aerogels became more compacted (densification), and their mechanical strengths, as demonstrated by stress-strain curves, gradually decreased for all nanofiber conditions (**Figure 6**a–d; Figures S5 and S6, Video S3, Supporting Information). However, no fracture was shown at any condition even after 10 000 cycles at a high strain above 80%, which clearly indicated their high mechanical durability.

More importantly, V_{OC}'s measured during 10 000 cycles explicitly demonstrated that the triboelectric output was well maintained at all conditions (Figure 6e–h; Figure S7, Supporting Information). This result was a clear indication that the densification and decreased mechanical strength did not lead to a structural loss, and there was no detrimental effect in triboelectric properties. Taken together, the nanofiber-AG provides a mechanically durable platform for stable long-term TENG performance.

2.4. Fabrication and Characterization of Wearable PSI-TENG

The characteristic mechanical properties of aerogels, such as lightweight, mechanical conformity and toughness, and shape recovery, make them highly suitable as a wearable TENG platform over other types of materials.[22,23,41,45] While traditional polymers used for aerogels generally lack triboelectric polarity, the strategy of incorporating "tribo-functional" PSI nanofibers was shown to substantially enhance the triboelectric

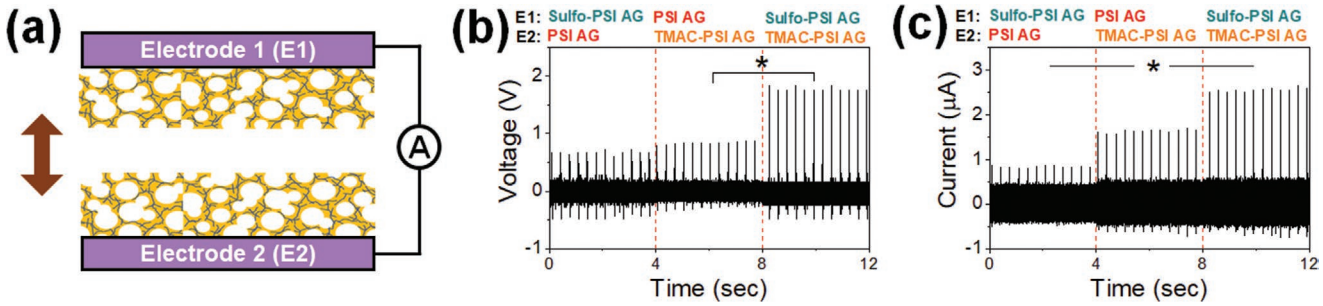

Figure 5. a) Schematic illustration of AG-only TENG in a contact-separation mode. Different nanofiber-AGs connected to electrodes (E1 and E2) were paired. b) Open-circuit voltage and c) short-circuit current values of PSI AG with Sulfo-PSI AG, PSI AG with TMAC-PSI AG, and Sulfo-PSI AG with AG (*$p < 0.05$ at $n = 10$ comparing different AG pairs). The concentration of nanofibers in the aerogel was 4%.

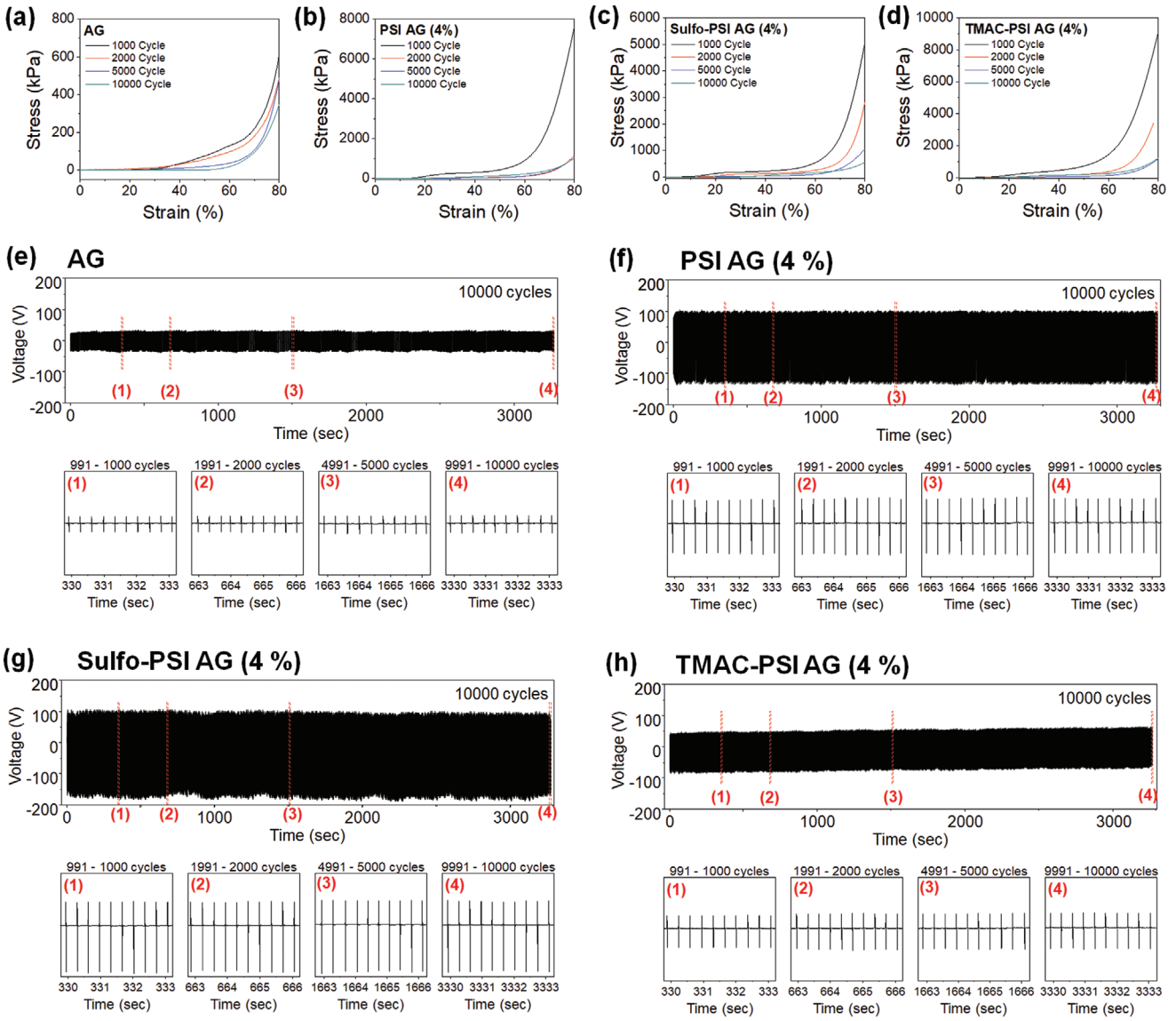

Figure 6. Mechanical durability of nanofiber-AG TENG was evaluated by measuring the stress–strain curve and triboelectric output (V_{OC}) via contact-separation operation up to 10 000 cycles: a,e) AG, b,f) PSI-AG, c,g) Sulfo-PSI AG, and d,h) TMAC-PSI AG. The nanofiber concentration was 4%. V_{OC} at four different ranges of operation cycles (1 to 4) are highlighted.

performance, while maintaining the favorable physicomechanical features of aerogel. Taking advantage of these attributes, the PSI nanofiber-AG TENG was utilized as a wearable energy harvester and motion sensor, which was integrated into an insole of a shoe (**Figure 7**a).[46–49] It was expected that varying triboelectric potentials would be generated in response to different movements such as walking and running. For this experiment, the TENG consisting of Sulfo-PSI AG and PFA as the triboelectric pair was assembled into a silicone shell, which was then embedded to an insole.

First, V_{OC} was measured from a TENG in one insole subjected to different stepping forces to confirm the ability to generate corresponding triboelectric potential (Figure 7b). As expected, higher V_{OC} was recorded from higher stepping force than lower stepping force. The signals were stably generated for a long period of time with repeated forces, demonstrating the mechanical durability and recoverability of the nanofiber-AG-based TENG. Interestingly, there was a larger time lag between the positive and negative V_{OC}'s during step on and step off. Since the area of contact was much wider, and the contact occurred more gradually during the stepping motion, the separation also occurred more gradually, resulting in the time lag.

Then, the wearable TENG's were integrated into both sides of the shoes and their triboelectric potentials were measured from walking and running. During walking (approximately 1 m s^{-1}), V_{OC}'s were recorded consistently and stably from both left and right shoes. However, the signal intensities and patterns were varied between left and right shoes and inconsistent even from one shoe, which was obviously due to the natural inconsistencies of a body motion (Figure 7c). These inconsistencies

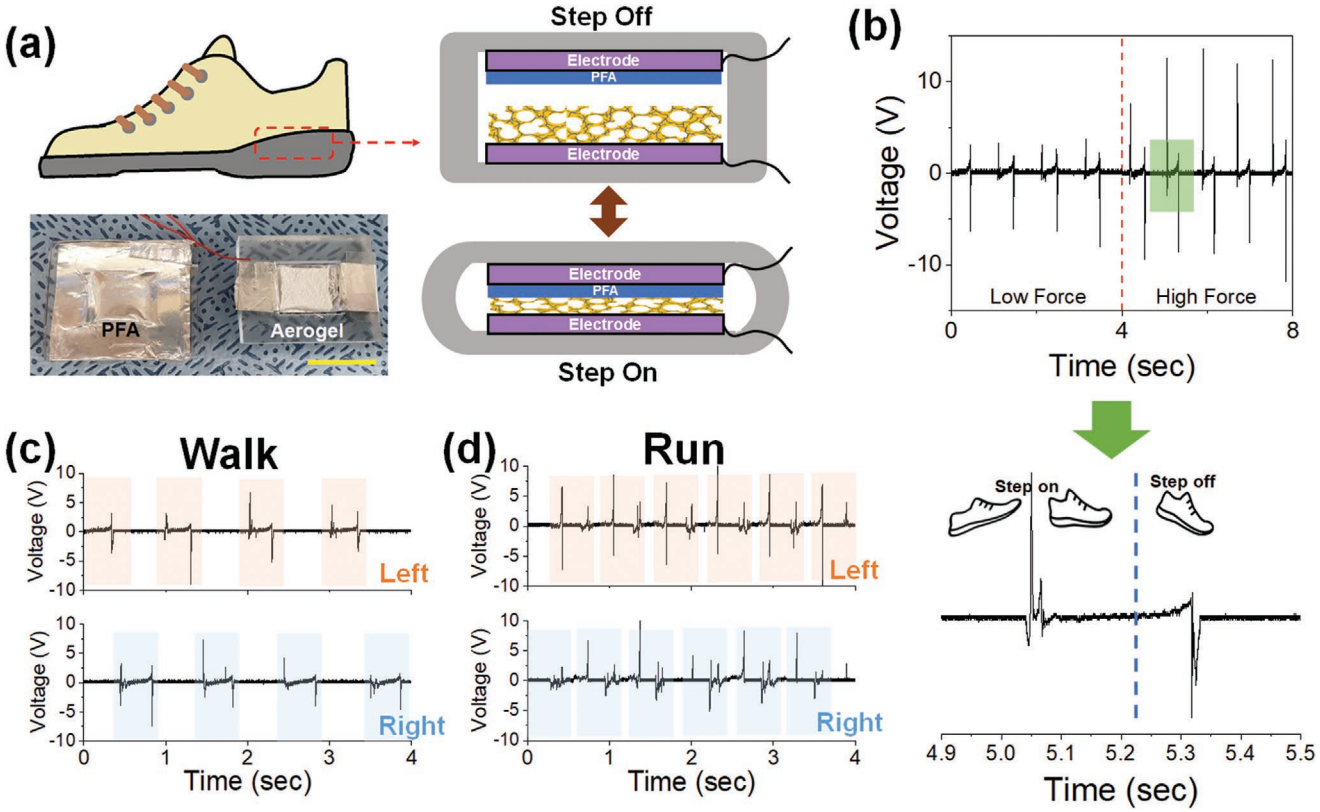

Figure 7. a) The schematic illustration and the photograph of a wearable TENG with Sulfo-PSI AG and PFA assembled into the insole of a shoe (scale bar: 5 cm). The contact-separation mode of the TENG would be operated during step on and step off. b) V_{OC} measured from a wearable Sulfo-PSI AG TENG via stepping with different forces. The graph on the bottom represents V_{OC} during a single step. c,d) V_{OC}'s measured from the wearable PSI-AG TENGs in both sides of the shoes during walking or running. Each highlighted area represents a single step on and off.

became more heightened with running (Figure 7d). The V_{OC} signals were sharper with greater intensities during step on, which was expected since the contact is stronger and faster during running (approximately 4 m s^{-1}). In addition, there was also a sharp, opposite V_{OC} immediately after initial positive V_{OC} from the left shoe, which was attributed to a stronger recoil upon initial contact. This recoil V_{OC} was not demonstrated and the overall intensities were lower from the right shoe. This difference was attributed to the imbalanced running gait of the test subject. Similarly, the V_{OC} signals became more turbulent with step off, which is also likely due to a more oscillatory motion during separation. Overall, in addition to energy harvesting, the triboelectric recordings generated from the wearable nanofiber-aerogel TENG during motion could be used as a wearable gait sensor for health monitoring, physical rehabilitation and sports science.[50]

3. Conclusion

This study presents a comprehensive engineering strategy for developing nanofiber-laden aerogel as a wearable TENG with highly tunable triboelectric performance. PSI allowed facile chemical functionalization via ring-opening nucleophilic addition, which was employed to conjugate anionic sodium sulfate or cationic trimethylammonium chloride, functional groups in order to tune the triboelectric polarity. The PSI and its derivatives were then fabricated into nanofibers for increased mechanical durability and contact area, which resulted in enhanced and tunable triboelectric properties. The nanofibers were then processed into a short, dispersible form and infused into a biocompatible alginate aerogel in order to impart and enhance triboelectric properties to a more mechanically durable and conformal material platform. The nanofiber-aerogel TENG was finally tested as a wearable sensor and energy harvester. Taken all together, the nanofiber-AG system introduced in this study is expected to provide a highly functional platform for a variety of wearable devices.

4. Experimental Section

Synthesis of Polysuccinimide (PSI): Polysuccinimide (PSI) was developed by polycondensation of aspartic acid.[21,27,51–53] Briefly, 50 g L-aspartic acid (Samchun Chemicals, South Korea) was dissolved in sulfone/mesitylene (45 mL/105 mL, Sigma-Aldrich). The reaction mixture was refluxed at 170 °C with mechanical stirring under dry N_2 for 5 h, and water formed during the reaction was continuously removed using a Dean-Stark trap. The crude product, which was precipitated out during reaction, was re-dissolved in dimethylformamide (Samchun Chemicals, South Korea), and precipitated in excess methanol. The product was washed several times with deionized (DI) water until the pH became neutral, and dried.

Derivatization of PSI: 1 g of PSI was first added to 10 mL dimethyl sulfoxide (Samchun Chemicals, South Korea). 2-aminoethyl sodium sulfate (Sulfo-NH_2) or (aminoethyl)trimethylammonium chloride (TMAC-NH_2) was added to the solution, and reacted for 24 h at 50 °C to synthesize Sulfo-PSI or TMAC-PSI, respectively. Detailed procedures for synthesizing Sulfo-NH_2 and TMAC-NH_2 are provided in the Supporting Information (Figure S1, Supporting Information).[54,55] The mixture was dialyzed extensively against DI water, and lyophilized to obtain the product. FT-IR (Model 670, Varian) and ^{1}H-NMR (400 MHz, Bruker) were used to confirm their characteristic chemical structures. Elemental analysis was also performed to quantify the presence of sulfur and nitrogen on Sulfo-PSI and TMAC-PSI, respectively (Flash 2000, Thermo Fisher).

Fabrication of PSI Nanofibrous Films: PSI (unmodified PSI, Sulfo-PSI, or TMAC-PSI) was dissolved in dimethylformamide at 30% w/v with ultrasonication (VCX130, Sonic). Electrospinning was used to generate PSI nanofibers (NanoNC, South Korea). The solution was loaded into a syringe with a 26 G needle, which was then assembled onto an electronic pump. The metal tip of the syringe needle and the collector was connected to a DC power supplier. The solution was ejected at a flow rate of 0.5 mL h^{-1}, while the voltage was applied at 23 kV. The distance between the needle tip to the collector was 15 cm. An acrylic plate (20 mm × 20 mm) coated with Al film (Coretech, South Korea), which would be used as the sample platform for triboelectric measurements, was placed on the collector. The nanofibers were collected for 30 min.

After nanofiber fabrication, the nanofiber mat was thermally annealed at 60 °C for 24 h. Then, it was further heat-pressed for 1 min to allow greater adhesion between the nanofiber and Al film. SEM was used to examine the detailed morphology of the nanofibers (S-4800, Hitachi).

Fabrication of Nanofiber-Laden Aerogel: 0.5% w/v sodium alginate (Sigma-Aldrich) was placed in a square mold (20 mm × 20 mm), and a filter paper was placed on top. The filter paper was soaked with 0.5% $CaCl_2$ solution, and allowed to sit for 1 h, during which the $CaCl_2$ solution diffused into the alginate solution, resulting in gelation. The alginate hydrogel was washed by immersing in excess DI water. The hydrogel was frozen using liquid N_2, and lyophilized to obtain aerogel.

To incorporate nanofiber into the aerogel, as-prepared PSI nanofiber mat developed via electrospinning was immersed in water. Ultrasonication was applied for 5 min in a pulse mode (5 s on, 5 s off, output power: 65 W, frequency: 20 kHz, VCX130, Sonic), resulting in micrometer-length, short nanofibers. These nanofibers were collected and dispersed in alginate solution at various concentrations; 1%, 2%, and 4% w/v. The aerogel was fabricated using the same method as described above. Inner morphology of nanofiber-laden aerogel was visualized with SEM (S-4800, Hitachi).

The mechanical properties of aerogels were evaluated by obtaining stress-strain curves via uniaxial compression (Model 3343, Instron). The elastic modulus was calculated as the slope at the initial 10% strain where the curve remained linear.

Triboelectric Output Measurement: TENG consisted of two Al-coated acrylic plates used as electrodes, one coated with perfluoroalkoxy alkane (PFA) (0.025 mm thickness, Alphaflon, Korea) film and the other coated with either PSI nanofibrous film or PSI nanofiber-laden aerogel as friction layers. Their active contact area was 4 cm^2 (20 mm × 20 mm). The thicknesses of the PSI nanofibrous film and the aerogel friction layer were 0.03 and 2 mm, respectively.

Triboelectric output signals were measured in a vertical contact-separation mode. The two plates were periodically pressed with a pushing tester (ET-126B-4 (electrodynamic transducer), pa-151 (power amplifier), Labworks Inc.) to apply the vertical force (30 N) at a frequency of 3 Hz. TENG electrodes were connected to a digital oscilloscope to monitor and measure the open-circuit voltage during experiment (Tektronix DPO 2014B Digital Phosphor). An ultra-low input current amplifier (LMC6001, Texas Instruments) was also used to generate and detect short-circuit current.[56] To evaluate the mechanical durability, the contact-separation operation was repeated up to 10 000 cycles, and the triboelectric output and stress–strain curves were obtained. Load resistance was varied from 100 KΩ to 10 MΩ, and the resulting output voltage and current were recorded, which were then used to calculate the output power.

Fabrication and Characterization of a Wearable TENG: Polydimethylsiloxane silicone (SYLGARD184, Dow Corning) mold was first fabricated, following the manufacturer's instruction, having the overall dimension of 10 cm × 10 cm × 2 cm and a shallow inner space (4 cm × 4 cm × 1 cm) in the middle. The Al electrode layers connected to electrical wires, PFA and Sulfo-PSI nanofiber-laden aerogel, fabricated as described above, were placed within the inner space. The schematic and photographic illustrations are provided in Figure 6. This wearable TENG was then inserted into an insole, which was then placed into a shoe. The changes in triboelectric signals in response to different motions were recorded. Since the device was embedded in the insole and there was not a direct contact made with any bodily part of the subject, the use of PSI-based TENG as a wearable gait sensor in this work did not meet the definition of human subject research at UNIST, therefore, IRB approval was not needed.

Statistical Analysis: Mean and standard deviation values from ten independent experiments were reported in this study for material characterization (n = 10). Statistical significance of differences between two conditions was assessed using Student's t-test. Statistical significance of difference between multiple conditions was evaluated by one-way ANOVA followed by Tukey's post hoc test (Microsoft Office Excel). p-values below 0.05 were considered statistically significant and are reported here.

Supporting Information

Supporting Information is available from the Wiley Online Library or from the author.

Acknowledgements

M.K., C.C., and J.P.L. contributed equally to this work. This study was supported by Basic Science Research Program and Leading Foreign Research Institute Recruitment Program funded by the Ministry of Science and ICT (2018R1D1A1B07048522, 2018K1A4A3A01063890), and Technology Innovation Program (or Industrial Strategic Technology Development Program) (20009198, Development and demonstration of biodegradable bioplastic prototype) funded by the Ministry of Trade, Industry & Energy (MOTIE, Korea).

Conflict of Interest

The authors declare no conflict of interest.

Data Availability Statement

The data that support the findings of this study are available on request from the corresponding author. The data are not publicly available due to privacy or ethical restrictions.

Keywords

aerogels, biosensors, nanofibers, polyaspartamide, triboelectric nanogenerators

Received: November 26, 2021
Revised: March 4, 2022
Published online: March 20, 2022

[1] Y.-M. Choi, M. G. Lee, Y. Jeon, *Energies* **2017**, *10*, 1483.
[2] Y. W. Chong, W. Ismail, K. Ko, C. Y. Lee, *IEEE Sens. J.* **2019**, *19*, 9047.
[3] A. Nozariasbmarz, H. Collins, K. Dsouza, M. H. Polash, M. Hosseini, M. Hyland, J. Liu, A. Malhotra, F. M. Ortiz, F. Mohaddes, V. P. Ramesh, Y. Sargolzaeiaval, N. Snouwaert, M. C. Özturk, D. Vashaee, *Appl. Energy* **2020**, *258*, 114069.
[4] H. Liu, J. Zhong, C. Lee, S.-W. Lee, L. Lin, *Appl. Phys. Lett.* **2018**, *5*, 041306.
[5] M. P. Kim, D.-S. Um, Y.-E. Shin, H. Ko, *Nanoscale Res. Lett.* **2021**, *16*, 35.
[6] H.-J. Yoon, H. Ryu, S.-W. Kim, *Nano Energy* **2018**, *51*, 270.
[7] Z. Liu, H. Li, B. Shi, Y. Fan, Z. L. Wang, Z. Li, *Adv. Funct. Mater.* **2019**, *29*, 1808820.
[8] A. Yu, Y. Zhu, W. Wang, J. Zhai, *Adv. Funct. Mater.* **2019**, *29*, 1900098.
[9] R. Zhang, H. Olin, *EcoMat* **2020**, *2*, e12062.
[10] H. Zou, Y. Zhang, L. Guo, P. Wang, X. He, G. Dai, H. Zheng, C. Chen, A. C. Wang, C. Xu, Z. L. Wang, *Nat. Commun.* **2019**, *10*, 1427.
[11] M. W. Williams, *AIP Adv.* **2012**, *2*, 010701.
[12] Y. Yu, X. Wang, *Extreme Mech. Lett.* **2016**, *9*, 514.
[13] H. Y. Li, L. Su, S. Y. Kuang, C. F. Pan, G. Zhu, Z. L. Wang, *Adv. Funct. Mater.* **2015**, *25*, 5691.
[14] Z. Peng, J. Song, Y. Gao, J. Liu, C. Lee, G. Chen, Z. Wang, J. Chen, M. K. H. Leung, *Nano Energy* **2021**, *85*, 106021.
[15] Q. Jing, S. Kar-Narayan, *J. Phys. D: Appl. Phys.* **2018**, *51*, 303001.
[16] M. Ibrahim, J. Jiang, Z. Wen, X. Sun, *Nanoenergy Adv.* **2021**, *1*, 58.
[17] X. Cheng, B. Meng, X. Chen, M. Han, H. Chen, Z. Su, M. Shi, H. Zhang, *Small* **2016**, *12*, 229.
[18] M.-L. Seol, J. - H. Woo, D. - I. Lee, H. Im, J. Hur, Y. - K. Choi, *Small* **2014**, *10*, 3887.
[19] M. N. Biutty, S. I. Yoo, *Macromol. Res.* **2021**, *29*, 98.
[20] K. Tanimoto, S. Saihara, Y. Adachi, Y. Harada, Y. Shiomi, Y. Tajitsu, *Jpn. J. Appl. Phys.* **2015**, *54*, 10NF02.
[21] E. Jalalvandi, A. Shavandi, *Eur. Polym. J.* **2018**, *109*, 43.
[22] H. Zhuo, Y. Hu, X. Tong, Z. Chen, L. Zhong, H. Lai, L. Liu, S. Jing, Q. Liu, C. Liu, X. Peng, R. Sun, *Adv. Mater.* **2018**, *30*, 1706705.
[23] H.-Y. Mi, X. Jing, M. A. B. Meador, H. Guo, L. - S. Turng, S. Gong, *ACS Appl. Mater. Interfaces* **2018**, *10*, 30596.
[24] L. Zheng, S. Zhang, Z. Ying, J. Liu, Y. Zhou, F. Chen, *Int. J. Nanomed.* **2020**, *15*, 2363.
[25] L. Dong, C. Xu, Y. Li, Z.-H. Huang, F. Kang, Q.-H. Yang, X. Zhao, *J. Mater. Chem. A* **2016**, *4*, 4659.
[26] H. Ryu, J.-H. Lee, T.-Y. Kim, U. Khan, J. H. Lee, S. S. Kwak, H.-J. Yoon, S.-W. Kim, *Adv. Energy Mater.* **2017**, *7*, 1700289.
[27] M. Tomida, T. Nakato, S. Matsunami, T. Kakuchi, *Polymer* **1997**, *38*, 4733.
[28] W. Wang, A. Yu, X. Liu, Y. Liu, Y. Zhang, Y. Zhu, Y. Lei, M. Jia, J. Zhai, Z. L. Wang, *Nano Energy* **2020**, *71*, 104605.
[29] H. Fong, I. Chun, D. H. Reneker, *Polymer* **1999**, *40*, 4585.
[30] X. Wei, Z. Xia, S.-C. Wong, A. Baji, *Int. J. Exp. Comput. Biomech.* **2009**, *1*, 45.
[31] A. Chen, C. Zhang, G. Zhu, Z. L. Wang, *Adv. Sci.* **2020**, *7*, 2000186.
[32] J. W. Lee, S. Jung, T. W. Lee, J. Jo, H. Y. Chae, K. Choi, J. J. Kim, J. H. Lee, C. Yang, J. M. Baik, *Adv. Energy Mater.* **2019**, *9*, 1901987.
[33] R. Zhang, M. Hummelgård, J. Örtegren, M. Olsen, H. Andersson, Y. Yang, H. Zheng, H. Olin, *Nano Energy* **2021**, *86*, 106041.
[34] T. Charoonsuk, S. Pongampai, P. Pakawanit, N. Vittayakorn, *Nano Energy* **2021**, *89*, 106430.
[35] X. Li, C. Jiang, Y. Ying, J. Ping, *Adv. Energy Mater.* **2020**, *10*, 2002001.
[36] A. Soleimani Dorcheh, M. H. Abbasi, *J. Mater. Process. Technol.* **2008**, *199*, 10.
[37] K. Ganesan, T. Budtova, L. Ratke, P. Gurikov, V. Baudron, I. Preibisch, P. Niemeyer, I. Smirnova, B. Milow, *Materials* **2018**, *11*, 2144.
[38] A. S. Jatoi, Z. Hashmi, S. A. Mazari, R. Abro, N. Sabzoi, *J. Porous Mater.* **2021**, *28*, 1919.
[39] J. Stergar, U. Maver, *J. Sol-Gel Sci. Technol.* **2016**, *77*, 738.
[40] H. Jin, Y. S. Abu-Raya, H. Haick, *Adv. Healthcare Mater.* **2017**, *6*, 1700024.
[41] S. Salimian, A. Zadhoush, M. Naeimirad, R. Kotek, S. Ramakrishna, *Polym. Compos.* **2018**, *39*, 3383.
[42] K. Lee, J. Hong, H. J. Roh, S. H. Kim, H. Lee, S. K. Lee, C. Cha, *Cellulose* **2017**, *24*, 4963.
[43] Q. Ye, Y. Wu, Y. Qi, L. Shi, S. Huang, L. Zhang, M. Li, W. Li, X. Zeng, H. Wo, X. Wang, S. Dong, S. Ramakrishna, J. Luo, *Nano Energy* **2019**, *61*, 381.
[44] R. D. I. G. Dharmasena, *Nano Energy* **2020**, *76*, 105045.
[45] Y. Zou, L. Bo, Z. Li, *Fundam. Res.* **2021**, *1*, 364.
[46] T. Huang, C. Wang, H. Yu, H. Wang, Q. Zhang, M. Zhu, *Nano Energy* **2015**, *14*, 226.
[47] M. He, W. Du, Y. Feng, S. Li, W. Wang, X. Zhang, A. Yu, L. Wan, J. Zhai, *Nano Energy* **2021**, *86*, 106058.
[48] D. Jiang, H. Ouyang, B. Shi, Y. Zou, P. Tan, X. Qu, S. Chao, Y. Xi, C. Zhao, Y. Fan, Z. Li, *InfoMat* **2020**, *2*, 1191.
[49] G. Q. Gu, C. B. Han, J. J. Tian, C. X. Lu, C. He, T. Jiang, Z. Li, Z. L. Wang, *ACS Appl. Mater. Interfaces* **2017**, *9*, 11882.
[50] S. M. A. Z. Shawon, A. X. Sun, V. S. Vega, B. D. Chowdhury, P. Tran, Z. D. Carballo, J. A. Tolentino, J. Li, M. S. Rafaqut, S. Danti, M. J. Uddin, *Nano Energy* **2021**, *82*, 105691.
[51] K. Matsubara, T. Nakato, M. Tomida, *Macromolecules* **1997**, *30*, 2305.
[52] J. Jang, C. Cha, *Biomacromolecules* **2018**, *19*, 691.
[53] M. Kim, C. Cha, *Biomacromolecules* **2020**, *21*, 3693.
[54] I. Yudovin-Farber, C. Yanay, T. Azzam, M. Linial, A. J. Domb, *Bioconjugate Chem.* **2005**, *16*, 1196.
[55] A. Nudelman, Y. Bechor, E. Falb, B. Fischer, B. A. Wexler, A. Nudelman, *Synth. Commun.* **1998**, *28*, 471.
[56] S. S. K. Mallineni, H. Behlow, R. Podila, A. M. Rao, *Nanotechnol. Rev.* **2018**, *7*, 149.